LA-UR- 09-06331

Approved for public release; distribution is unlimited.

Title:	The Electrosphere of Macroscopic "Nuclei": Diffuse Emissions in the MeV Band from Dark Antimatter
Author(s):	Michael Forbes, T-2 Kyle Lawson, Ariel r. Zhitnitsky, Univ. of British Columbia
Intended for:	Physical Review D

Los Alamos NATIONAL LABORATORY EST. 1943

The Electrosphere of Macroscopic "Nuclei": Diffuse Emissions in the MeV Band from Dark Antimatter.

$Revision : 2355,\ Date : 2009 - 09 - 1113 : 37 : 21 - 0600(Fri, 11Sep2009)$

Michael McNeil Forbes*
T-2 Division, Los Alamos National Laboratory, Los Alamos, NM, 87545, USA

Kyle Lawson and Ariel R. Zhitnitsky
Department of Physics and Astronomy, University of British Columbia, Vancouver, BC, V6T 1Z1, Canada

(Dated: September 11, 2009)

Using a Thomas-Fermi model, we calculate the structure of the electrosphere of the quark antimatter nuggets postulated to comprise much of the dark matter. This provides a single self-consistent density profile from ultra-relativistic densities to the non-relativistic Boltzmann regime. We use this to present a microscopically justified calculation of several properties of the nuggets, including their net charge, and the ratio of MeV to 511 keV emissions from electron annihilation. We find that the calculated parameters agree with previous phenomenological estimates based on the observational supposition that the nuggets are a source of several unexplained diffuse emissions from the galaxy. This provides another nontrivial verification of the dark matter proposal. The structure of the electrosphere is quite general and will also be valid at the surface of strange-quark stars, should they exist.

PACS numbers:

Contents

I. Introduction 1

II. Dark Matter as Dense Quark Nuggets 2

III. Electrosphere Structure 4
- A. Thomas-Fermi Model 4
  - 1. Boundary Conditions 4
- B. Profiles 5
- C. Nugget Charge Equilibrium 6

IV. Diffuse Galactic Emissions 8
- A. Observations 8
  - 1. The 511 keV Line 8
  - 2. Diffuse MeV scale emission 8
  - 3. Comparison 9
- B. Annihilation rates 9
  - 1. Positronium Formation 9
  - 2. Direct Annihilation Rates 9
- C. Spectrum and Branching Fraction 10
  - 1. Normalization to the 511 keV line 11

V. Conclusion 12

Acknowledgments 12

References 12

A. Density Functional Theory 14
  - 1. Thomas-Fermi Approximation. 14
  - 2. Analytic Solutions 14
    - a. Ultra-Relativistic Regime 14
    - b. Boltzmann Regime 15
  - 3. Numerical Solutions 15

B. Debye Screening In the Electrosphere 17

I. INTRODUCTION

In this paper we explore some details of a testable and well-constrained model for dark matter [1–5] in the form of quark matter as antimatter nuggets. In particular, we focus on physics of the "electrosphere" surrounding these nuggets: It is from here that observable emissions emanate, allowing for the direct detection of these dark antimatter nuggets.

We first provide a brief review of our proposal in section II, then describe the structure of the electrosphere of the nuggets using a Thomas-Fermi model in section III. This allows us to calculate the charge of the nuggets, and to discuss how they maintain charge equilibrium with the environment. We then apply these results to the calculation of emissions from electron annihilation in section IV, computing some of the phenomenological parameters introduced in [6]. The computed values of the parameters are consistent with the values required to explain current observations, providing further validation of our model for dark matter. The present results concerning the density profile of the electrosphere may also play an important role in the study of the surface of quark stars, should they exist.

*E-mail: mforbes@alum.mit.edu

II. DARK MATTER AS DENSE QUARK NUGGETS

Two of the outstanding cosmological mysteries – the natures of dark matter and baryogenesis – might be explained by the idea that dark matter consists of Compact Composite Objects (CCOs) [1–5] similar to Witten's strangelets [7]. The basic idea is that these CCOs – nuggets of dense matter and antimatter – form at the same QCD phase transition as conventional baryons (neutrons and protons), providing a natural explanation for the similar scales $\Omega_{\text{DM}} \approx 5\Omega_{\text{B}}$. Baryogenesis proceeds through a charge separation mechanism: both matter and antimatter nuggets form, but the natural CP violation of the so-called θ term in QCD[1] – which was of order unity $\theta \sim 1$ during the QCD phase transition – drives the formation of more antimatter nuggets than matter nuggets, resulting in the leftover baryonic matter that forms visible matter today (see [2] for details). Note, it is crucial for our mechanism that CP violation can drive charge separation. This idea may already have found experimental support through the Relativistic Heavy Ion Collider (RHIC) at Brookhaven [18].

The mechanism requires no fundamental baryon asymmetry to explain the observed matter/antimatter asymmetry. Together with the observed relation $\Omega_{\text{DM}} \approx 5\Omega_{\text{B}}$ (see [19] for a review) we have

$$B_{\text{universe}} = 0 = B_{\text{nugget}} + B_{\text{visible}} - \bar{B}_{\text{antinugget}} \tag{1a}$$

$$B_{\text{dark-matter}} = B_{\text{nugget}} + \bar{B}_{\text{antinugget}} \approx 5B_{\text{visible}} \tag{1b}$$

where B_{universe} is the overall baryon asymmetry – the total number of baryons *minus* antibaryons in the universe – and $B_{\text{dark-matter}}$ is the total number of baryons *plus* antibaryons hidden in the dark matter nuggets. The dark matter comprises B_{nugget} baryons contained in matter nuggets and $\bar{B}_{\text{antinugget}}$ antibaryons contained in antimatter nuggets. The remaining B_{visible} baryons are not confined and form the residual "visible" baryon excess that forms the regular matter in our universe today. Solving equations (1) gives the approximate ratios $\bar{B}_{\text{antinugget}}:B_{\text{nugget}}:B_{\text{visible}} \simeq 3:2:1$.

Unlike conventional dark matter candidates, dark-matter/antimatter nuggets will be strongly interacting, but macroscopically large objects. They do not contradict any of the many known observational constraints on dark matter or antimatter [3, 20] for three reasons:

1. They carry a huge (anti)baryon charge $|B| \approx 10^{20}$ – 10^{33}, so they have an extremely tiny number density.[2] This explains why they have not been directly observed on earth. The local number density of dark-matter particles with these masses is small enough that interactions with detectors are exceedingly rare and fall within all known detector and seismic constraints [3]. (See also [21, 22] and references therein).

2. The nuggets have nuclear densities, so their interaction cross-section is small $\sigma/M \approx 10^{-13}$-$10^{-9}$ cm^2/g: well below the typical astrophysical and cosmological limits which are on the order of $\sigma/M < 1$ cm^2/g. Dark-matter–dark-matter interactions between these nuggets are thus negligible.

3. They have a large binding energy such that baryons in the nuggets are not available to participate in big bang nucleosynthesis (BBN) at $T \approx 1$ MeV. In particular, we suspect that the baryons in these nuggets form a superfluid with a gap of the order $\Delta \approx 100$ MeV, and critical temperature $T_c \sim \Delta/\sqrt{2} \approx 60$ MeV, as this scale provides a natural explanation for the observed photon to baryon ratio $n_B/n_\gamma \sim 10^{-10}$ [2], which requires a formation temperature of $T_{\text{form}} = 41$ MeV [23].[3]

Thus, on large scales, the nuggets are sufficiently dilute that they behave as standard collisionless cold dark matter (CCDM). When the number densities of both dark and visible matter become sufficiently high, however, dark-antimatter–visible-matter collisions may release significant radiation and energy. In particular, antimatter nuggets provide a site at which interstellar baryonic matter – mostly protons and electrons – can annihilate, producing emissions with calculable spectra and energies that should be observable from the core of our Galaxy. These emissions are not only consistent with current observations, but naturally explain several mysterious diffuse emissions observed from the core of our Galaxy, with frequencies ranging over 12 orders of magnitude.

Although somewhat unconventional, this idea naturally explains several coincidences, is consistent with all known cosmological constraints, and makes testable predictions. Furthermore, this idea is almost entirely rooted in conventional and well-established physics. In particular, there are no "free parameters" that can be – or need

[1] If θ is nonzero, one must confront the so-called strong CP problem whereby some mechanism must be found to make the effective θ parameter extremely small today in accordance with measurements. This problem remains one of the most outstanding puzzles of the Standard Model, and one of the most natural resolutions is to introduce an axion field. (See the original papers [8], [11], [13], and recent reviews [15].) Axion domain walls associated with this field (or ultimately, whatever mechanism resolves the strong CP problem) play an important role in forming these nuggets, and may play in important role in their ultimate stability. See [1, 2] for details.

[2] If the average nugget size ends up in the lower range, then the Pierre Auger observatory may provide an ideal venue for searching for these dark-matter candidates.

[3] At temperatures below the gap, incident baryons with energies below the gap would Andreev reflect rather than become incorporated into the nugget.

to be – "tuned" to explain observations: In principle, everything is calculable from well-established properties of QCD and QED. In practice, fully calculating the properties of these nuggets requires solving the fermion many-body problem at strong coupling, so we have generally resorted to "fitting" a handful of phenomenological parameters from observations. In this paper we examine the QED physics of the electrosphere, providing a microscopic basis for some of these parameters.

Once these parameters are determined, the model makes unambiguous predictions about other processes ranging over more than 10 orders of magnitude in scale. The basic picture involves the antimatter nuggets - compact cores of nuclear or strange quark matter surrounded by a positron cloud with a profile as calculated in section III. Incident matter will annihilate on these nuggets producing radiation at a rate proportional to the annihilation rate, thus scaling as the product $\rho_V(r)\rho_{DM}(r)$ of the local visible and dark matter densities. This will be greatest in the core of the galaxy. To date, we have considered five independent observations of diffuse radiation from the core of our Galaxy:

1. SPI/INTEGRAL observes 511 keV photons from positronium decay that is difficult to explain with conventional astrophysical positron sources [24–26]. Dark-antimatter nuggets would provide an unlimited source of positrons as suggested in [27, 28].

2. COMPTEL detects a puzzling excess of 1–20 MeV γ-ray radiation. It was shown in [6] that the direct e^+e^- annihilation spectrum could nicely explain this deficit, but the annihilation rates were crudely estimated in terms of some phenomenological parameters. In this paper we provide a microscopic calculation of these parameters (Eqs. (19) and (21)), thereby validating this prediction.

3. *Chandra* observes a diffuse keV X-ray emission that greatly exceeds the energy from identified sources [29]. Visible-matter/dark-antimatter annihilation would provide this energy. It was shown in [4] that the intensity of this emission is consistent with the 511 keV emission if the rate of proton annihilation is slightly suppressed relative to the rate of electron annihilation. In section III C we describe the microscopic nature of this suppression.

4. EGRET/CRGO detects MeV to GeV gamma-rays, constraining antimatter annihilation rates. It was shown in [4] that these constraints are consistent with the rates inferred from the other emissions.

5. WMAP has detected an excess of GHz microwave radiation – dubbed the "WMAP haze" – from the inner 20° core of our Galaxy [30–34]. Annihilation energy not immediately released by the above mechanisms will thermalize, and subsequently be released as thermal bremsstrahlung emission at the eV scale. In [5] it was shown that the predicted emission from the antimatter nuggets is consistent with, and could completely explain, the observed WMAP haze.

These emissions arise from the following mechanism: Neutral hydrogen from the interstellar medium (ISM) will easily penetrate into the electrosphere, providing a source of electrons an protons. The first and simplest process is the annihilation of the electrons through positronium formation, producing 511 keV photons as discussed in [27, 28]. Our proposal can easily explain the observed 511 keV radiation, and if we assume that this process is the dominant source, then we can use this to normalize the intensities of the other emissions. One of the remarkable features of this proposal is that it predicts the correct intensity for all of the other observations, even though they span many orders of magnitude in frequency.

The second process is direct annihilation of the electrons on the positrons in the electrosphere. As discussed in appendix B, the electrons are strongly screened by the positron background, and some fraction can penetrate deep within the electrosphere. There they can directly annihilate with high momentum positrons in the Fermi sea producing radiation up to 10 MeV or so. This process was originally discussed in [6] where the ratio of direct MeV annihilation to 511 keV annihilation was characterized by several phenomenological parameters who's values were chosen to fit the observations. In section IV we put this prediction on solid ground and show that these values agree with the microscopic calculation based on the electrosphere structure, which depends only on QED.

The other radiation originates from the energy deposited by annihilation of the incident protons in the core of the nuggets. In [4] we argue that the protons will annihilate just inside the surface of the core, releasing some 2 GeV of energy. Occasionally this process will release GeV photons – the rate of which is consistent with the EGRET/CRGO constraints – but most of the energy will be transferred to strongly interacting components, and ultimately about half will scatter down into $\sim$ 5 MeV positrons that stream out of the core. (The 5 MeV scale comes from the effective mass of the photon in the medium which mediates the energy exchange). These positrons are accelerated by the strong electric fields, and emit field-induced Bremsstrahlung emission in the 10 keV band – a scale set by balancing the rate of emission with the local plasma frequency (photons can only be emitted once the plasma frequency is low enough). The spectrum is also calculable: It is very flat and similar to a thermal spectrum without the sharp falloff above the temperature scale. This is consistent with the *Chandra* observations which cannot resolve the thermal falloff, but future analysis might be able to distinguish between the two.

We shall shed some light on the interaction between the protons and the core in section III C, but cannot yet perform the required many-body analysis to place all of this on a strong footing as this would require a practical solution to outstanding problems of high-density QCD.

The remaining energy will thermalize within the nuggets, until an equilibrium temperature of about $T \sim 1$ eV is reached [5]. Direct thermal emission at this scale would be virtually impossible to see against the backgrounds, but the spectrum – calculable entirely from QED – extends to very low frequencies, and the intensity of the emission in the microwave band is just enough to explain the WMAP haze [5].

III. ELECTROSPHERE STRUCTURE

Here we discuss the density profile of the electron cloud surrounding extremely heavy macroscopic "nuclei". We present here a type of Thomas-Fermi analysis including the full relativistic electron equation of state required to model the relativistic regime close to the nuclear core. We consider here the limit when the temperature is much smaller than the mass $T \ll 511$ MeV. The solution for higher-temperatures follows from similar techniques with fewer complications.

The observable properties of the antimatter nuggets discussed so far [1–6] depend on the existence of a non-relativistic "Boltzmann" regime with a density dependence $n(r) \sim (r - r_B)^{-2}$ (see appendix 1 of Ref. [5] for details). This region plays an important role in explaining the WMAP haze [5] as well as in the analysis of the diffuse 511 keV emissions [2]. The techniques previously used, however, were not sufficient to connect this non-relativistic "Boltzmann" regime to the relativistic regime through a self-consistent solution determined by parameters T, μ, m_e.

The main point of this section is to put the existence of a sizable Boltzmann regime on a strong footing, and to calculate some of the previously estimated phenomenological parameters that depend sensitively on density profile. These may now be explicitly computed from QED using a justified Thomas-Fermi approximation to reliably account for the many-body physics. We show that, indeed, a sizable Boltzmann regime exists for all but the smallest nuggets which are ruled out by lack of terrestrial detection observation. We also address the question of how the nuggets achieve charge equilibrium (section III C), discussing briefly the charge exchange mechanism, and determining the overall charge (see Table I).

A. Thomas-Fermi Model

To model the density profile of the electrosphere, we use a Thomas-Fermi model for a Coloumb gas of positrons. This is derivable from a density functional theory (see Appendix A) after neglecting the exchange contribution, which is suppressed by the weak coupling α. The electrostatic potential $\phi(r)$ must satisfy the Poisson equation

$$\nabla^2\phi(r) = -4\pi e n(r). \tag{2}$$

where $en(r)$ is the charge density. We express everything in terms of the local effective chemical potential

$$\mu(r) = \mu - V_{\text{eff}}(r) = \mu - e\phi(r) - V_{\text{ext}}(r). \tag{3}$$

and express the local charge density through the function $q(r) = en[\mu(r)]$ where $n[\mu]$ contains all of the information about the equation of state, including the finite temperature effects.

The external potential $V_{\text{ext}}(r)$ will be established by the nuclear-matter core, and will be zero outside. We shall implement this as a boundary condition at the core boundary $r = R$, and thus only consider the region $r > R$ where $V_{\text{ext}}(r) = 0$. The resulting solution may thus be expressed in terms of the equations

$$\nabla^2\mu(r) = 4\pi\alpha n[\mu(r)], \quad \epsilon_p = \sqrt{p^2 + m^2} \tag{4a}$$

$$n[\mu] = 2\int \frac{\mathrm{d}^3p}{(2\pi)^3}\left[\frac{1}{1 + e^{(\epsilon_p - \mu)/T}} - \frac{1}{1 + e^{(\epsilon_p + \mu)/T}}\right], \tag{4b}$$

with the appropriate boundary conditions at $r = R$ and $r = \infty$. In (4b) we have explicitly included both particle and antiparticle contributions, the spin degeneracy factor, and have used modified Planck units where $\hbar = c = 4\pi\epsilon_0 = 1$ so that $e^2 = \alpha$ and energy, momentum, inverse distance and inverse time are expressed in eV.

We assume spherical symmetry so that we can express

$$\nabla^2\mu(r) = \frac{1}{r^2}\frac{\mathrm{d}}{\mathrm{d}r}r^2\frac{\mathrm{d}}{\mathrm{d}r}\mu(r) = \mu''(r) + 2\mu'(r)/r. \tag{5}$$

Close to the surface of the nuggets, the radius is sufficiently large compared with the relevant length scales that the curvature term $2\mu'(r)/r$ may be neglected. We shall call the resulting approximation "one-dimensional". The resulting profile does not depend on the size of the nuggets and remains valid until the electrosphere extends to a distance comparable to the radius of the nugget, at which point the full three-dimensional form will cut-off the density. When applied to the context of strange stars [35–38], the one-dimensional approximation will be completely sufficient.

To help reason about the three-dimensional equation, we note that (4a) may be expressed as

$$\mu''(x) = x^{-4}4\pi\alpha n[\mu(x)] \tag{6}$$

where $x = 1/r$. A nice property of this transformation is that $\mu(x)$ must be a convex function if the charge density has the same sign everywhere.

1. Boundary Conditions

The physical boundary condition at the origin follows from smoothness of the potential. With this and an appropriate long-distance boundary-condition, one could in principle model the entire distribution of electrons throughout the core with an external potential $V_{\text{ext}}(r)$ established by the quark-matter.

In the nuclear matter core, however, beta-equilibrium essentially establishes a chemical potential on the order of 10 − 100 MeV [35] that depends slightly on the exact equation of state for the quark-matter phase (which is not known). Thus, we may simply take the boundary condition as $\mu(R) = \mu_R \approx 25$ MeV. Our results are not very sensitive to the exact value, though if less that 20 MeV, then this acts as a cutoff for the direct e^+e^- emission discussed in Section IV A 2.

The formal difficulty in this problem is properly formulating the long-distance boundary conditions. At $T = 0$, the large-distance boundary condition for non-relativistic systems is clear: $n(r \to \infty) = 0$. From (6) we see that $\mu(x)$ is linear with slope $-eQ$ where Q is the overall charge of the system (ions with a deficiency of electrons/positrons are permitted in the theory, see for example [39]):

$$eQ(r) = \int_0^r \mathrm{d}r\; 4\pi\alpha n(r)r^2 = \int_0^r \mathrm{d}r\; \left(r^2\mu'(r)\right)' = r^2\mu'(r).$$

At finite temperature, however, this type of boundary-condition is not appropriate. Instead, one must consider how equilibrium is established with the environment.

In a true vacuum, a finite temperature nugget will "radiate" the loosely bound outer electrosphere until the electrostatic potential is comparable to the temperature $eQ/r_* \sim T$. At this point, the rate of radiation starts to be exponentially suppressed. Suppose that the density at this point is $n(r_*)$. We can estimate an upper bound for the evaporation rate as $4\pi r_*^2 vn$ where $v \sim \sqrt{T/m}$.[4]

This needs to be compensated by rate of charge deposition from the surrounding plasma which can be estimated as $4\pi R^2 v_{N^+,\text{ISM}} n_{N^+,\text{ISM}}$ where $v_{N^+,\text{ISM}} \sim 10^{-3}c$ is the typical relative speed of the nuggets and charged components in the Inter-Stellar Medium (ISM). The density $n_{N^+,\text{ISM}}$ of charged components in the core of the galaxy is typically 10^{-1} to 10^{-2} of the total density $n_{\text{ISM}} \sim 1\ \text{cm}^{-3}$. (See also Section III C). Thus, once the density falls below

$$n < n_{\text{rad}} \sim \frac{R^2}{r^2}\sqrt{\frac{m}{T}} v_{N^+,\text{ISM}} n_{\text{ISM}} 10^{-2} \tag{7}$$

charge equilibrium can easily be established. This allows us to formulate the long-distance boundary conditions by picking a charge Q and outer radius r_* such that $eQ/r_* \sim T$, and $n(r_*) \sim n_{\text{rad}}$, establishing both the typical charge of the nuggets as well as the outer boundary condition for the differential equation (4).[5]

Note that the Thomas Fermi approximation is not trust-worthy in these regimes of extremely low density, but the boundary condition suffices to provide an estimate of the charge of the nuggets: were they to be less highly charged, then density at r_* would be sufficiently high that evaporation would increase the charge; were they more highly charged, then the evaporation rate would be exponentially suppressed.

Thus, for the antimatter nuggets, the density profile is determined by system (4) and the boundary conditions

$$\mu(R) = \mu_R \sim 25\ \text{MeV}, \tag{8a}$$

$$eQ/r_* = T \sim 1\ \text{eV}, \quad n(r_*) = n_{\text{rad}}(r_*). \tag{8b}$$

B. Profiles

In principle, one should also allow the temperature to vary, but recall that the rate of radiation in the Boltzmann regime is suppressed by almost six orders of magnitude with respect to the black-body scale while the density of the plasma $n_B \sim (mT)^{3/2}$ is quite large [5]. Thus, the abundance of excitations ensures that the thermal conductivity is high enough that an essentially constant temperature is maintained throughout the electrosphere.

One can now numerically solve the system (4) and (8). We shall consider six cases: total (anti)baryon charge $B \in \{10^{20}, 10^{24}, 10^{33}\}$ and quark matter densities $n_{\text{core}} \in \{1, 100\}\ \text{fm}^{-3}$. The resulting profiles are plotted in Fig. 1.[6] As a reference, we also plot the "one-dimensional" approximation obtained numerically by neglecting the curvature term in (5) as well as two analytic approximations: One for the ultra-relativistic regime [35, 36, 41][7] where $n[\mu] \approx \mu^3/3\pi^2$:

$$n_{\text{UR}}(z) \approx \frac{\mu_R^3}{3\pi^2(1 + z/z_{\text{UR}})^3}, \qquad z_{\text{UR}} = \mu_R^{-1}\sqrt{\frac{3\pi}{2\alpha}}, \tag{9}$$

and one for the non-relativistic Boltzmann regime [5] where $n[\mu] \propto e^{\mu/T}$:

$$n_B(z) = \frac{T}{2\pi\alpha}\frac{1}{(z + z_B)^2}. \tag{10}$$

Since we have the full density profiles, we fit z_B here so that the this approximation matches the numerical solution at $n_B = (mT/2\pi)^{3/2}$, (a slightly better approximation than used in [5]).

[4] The Boltzmann averaged velocity is lower $\langle v\rangle = \sqrt{T/(2\pi m)}$, and cutting off the integral properly will lower this even more, so this gives a conservative upper bound on the evaporation rate.

[5] Strictly speaking, at finite T the equations do not have a formal solution with a precise total charge because there is always some density for $\mu > 0$, however, practically, once $m - \mu \ll T$, the density will become exponentially small and so the charge is practically fixed.

[6] Note that the ultra-relativistic approximation employed in [40] not only overestimates the density by 3 orders of magnitude in the Boltzmann regime, but also has a different z-dependence ((9) verses (10)): The ultra-relativistic approximation is *not* valid for $\mu < m$ where most of the relevant physical processes take place.

[7] For $T \neq 0$, see appendix A 2 a.

B	$n_{\rm core}$	R	Q
10^{20}	$100\ {\rm fm}^{-3}$	10^{-7} cm	$5\times10^{1}e$
	$1\ {\rm fm}^{-3}$	5×10^{-7} cm	$2\times10^{2}e$
10^{24}	$100\ {\rm fm}^{-3}$	2×10^{-6} cm	$10^{3}e$
	$1\ {\rm fm}^{-3}$	10^{-5} cm	$4\times10^{3}e$
10^{33}	$100\ {\rm fm}^{-3}$	2×10^{-3} cm	$10^{6}e$
	$1\ {\rm fm}^{-3}$	10^{-2} cm	$4\times10^{6}e$

TABLE I: Antimatter nugget properties: the core radius R and total electric charge Q for nuggets with two different assumed core densities $n_{\rm core}$ and three different anti-baryon charges B. These correspond to the profiles shown in Fig. 1.

All of our previous estimates about physical properties of the antimatter nuggets – emission of radiation, temperature etc. – have been based on these approximations using the region indicated in Fig. 1, it is clear that they work very well, *as long as these regimes exist.* The potential problem is that the nuggets could be highly charged or sufficiently small that the one-dimensional Boltzmann regime fails to exist with the density rapidly falling through the relevant density scales. We can see from the results in Fig. 1 that the non-relativistic region exists for all but the smallest nuggets: As long as $B > 10^{20}$ – as required by current detector constraints [4] – then the one-dimensional approximation suffices to calculate the physical properties.

The annihilation rates discussed in section IV have also been included in Fig. 1 to show that these effects only start once the densities have reached the atomic density scale which is higher than the Boltzmann regime. Thus these results are also insensitive to the size of the nugget and the domain-wall approximation suffices. It is clear that one must have a proper characterization of the entire density profile from non-relativistic through to ultra-relativistic regimes in order to properly calculate the emissions: one cannot use the simple analytic forms.

We now discuss how charge equilibrium is established, and then apply our results to the fix the relative normalization between the diffuse 1 – 20 MeV emissions and the 511 keV emissions from the core of our galaxy. As we shall show, the relative normalization is now firmly rooted in conventional physics, and in agreement with the previous phenomenological estimate [6], providing another validation of our theory for dark matter.

C. Nugget Charge Equilibrium

In order to determine the effective charge of the nuggets we must consider how equilibrium is obtained. For the matter nuggets, equilibrium is established through essentially static equilibrium with the surrounding ISM plasma, however, for the antimatter nuggets, no such static equilibrium can be achieved. Instead, one must consider the dynamics of the following charge exchange processes:

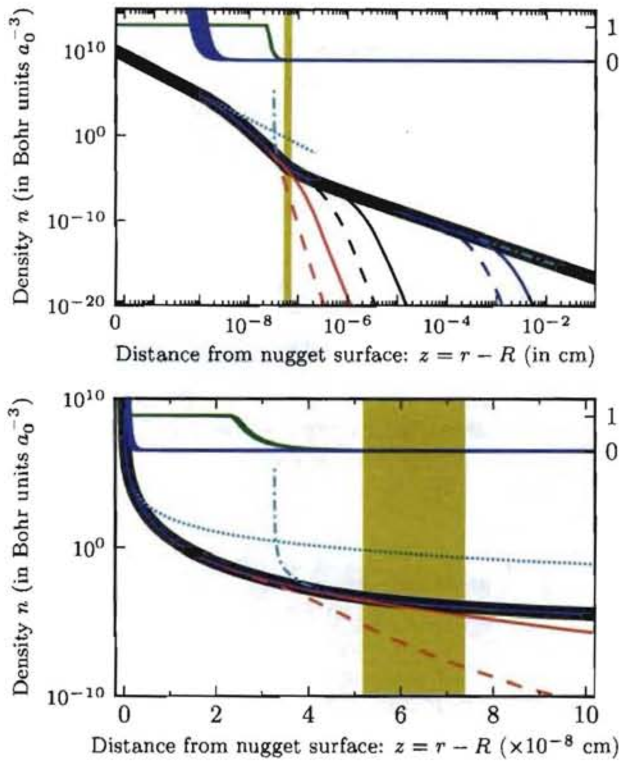

FIG. 1: (Colour online) Density profile of antimatter nuggets with baryon charge $B = 10^{20}$ (red), 10^{24} (black) and 10^{33} (blue) from left to right respectively assuming both nuclear density cores (solid lines) and 100 times nuclear density (dashed lines). The thick line is the one-dimensional approximation neglecting the curvature of the nugget and the shaded (yellow) regions correspond to the non-relativistic Boltzmann regime from which the diffuse microwave emissions [5] occur and where the Boltzmann approximation (10) (cyan dash-dotted line) is valid. The upper curves are the annihilation rates Γ_{Ps} (green, right) and $\Gamma_{\rm dir}$ (blue, left) normalized to the saturated value $\Gamma_{Ps}(\mu=\infty) = 4vq^3/(3\pi m^2\alpha^2)$ (12) (axis on right). These curves comprise a range of cutoffs $q \sim m\alpha$ such the positronium annihilation rates (12) vary by 10%, and a range of incoming velocities $10^{-3}c < v < 10^{-2}c$. The scaling of the abscissa in the upper figure is $\ln(z + z_{\rm UR})$ where $z_{\rm UR} \approx 5\times10^{-11}$ so that the $T = 0$ ultra-relativistic approximation (9) is linear (finely dotted cyan line). The abscissa are linearly spaced in the bottom figure.

1. Deposition of charge via interaction and annihilation of neutral ISM components (primarily of neutral hydrogen).

2. Deposition of charge via interaction and annihilation of ionized ISM components (primarily electrons and protons.)

3. Thermal evaporation of positrons from antinugget's surface.

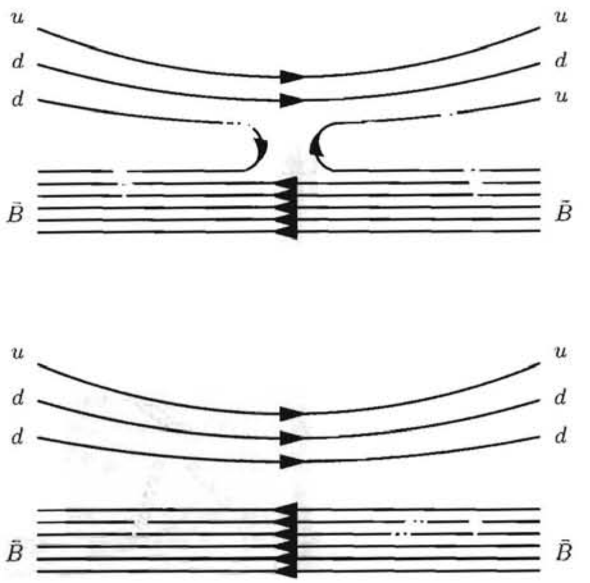

FIG. 2: Charge exchange process (top diagram): A charged incoming proton (upper left) exchanges a down quark d for an up quark u with the antimatter nugget $\bar{B}$, reflecting as a neutron (upper right). This is Zweig suppressed relative to the simple reflection process illustrated below, however, the neutron can escape from the system whereas the reflected proton will be trapped by the electric fields. This will enhance the overall rate of charge exchange reactions because the proton will continue to react again and again until either the charge exchange occurs, or it eventually annihilates. In order to explain the relative intensities of the observed 511 keV and diffuse x-ray emissions from the core of our galaxy [4], the ratio of the charge exchange rate to the annihilation rate must be $f \sim 0.1$–0.5. To calculate this from microscopic physics, however, requires details of the nugget surface that are not yet known. Perhaps some model-insensitive estimates could be made, which would provide a highly non-trivial test of our theory based on microscopic physics.

First we consider an impinging neutral atom or molecule with velocity $v_{N,\text{ISM}} \sim 10^{-3}c$. Even if the antinugget is charged, these are neutral and will still penetrate into the electrosphere. Here the electrons will annihilate leaving a positively charge nucleus with energy $T_{\text{ISM}} \sim \frac{1}{2}m_N v_{N,\text{ISM}}^2$. As the electrosphere consists of positrons, this charge cannot be screened, so the nucleus will accelerate to the core. At the core the nucleus will either penetrate and annihilate, resulting in the diffused x-ray emissions discussed in [4] and providing the heat to fuel the microwave emissions [5], or will bounce off of the surface due to the sharp quark-matter interface.[8]

Note that, if the nuggets are sufficiently charged such that kinetic energy of the incoming nucleus at the point of ionization is smaller than the electrostatic energy,

$$T_{\text{ISM}} \sim \tfrac{1}{2}m_N v_{N,\text{ISM}}^2 \sim \text{eV} \ll \frac{eQ}{r} \sim \text{keV} \sim 10^7 \text{ K}, \quad (11)$$

then the charged nucleus will be unable to escape and will return to the core to either annihilate or undergo a charge exchange reaction to become neutral, after which it may leave unimpeded by the electric field. For nuggets with $B \sim 10^{20}$, 10^{24}, and 10^{33} respectively, this critical charge is $Q/e \gg 1$, 10^2, and 10^4 respectively. As shown in Table I, the charge established through evaporation greatly exceeds this critical charge, so the charged nucleus will not be able to escape the antinugget unless it undergoes a charge-exchange reaction (see Fig. 2).

For a single proton, such a charge-exchange reaction consists of an up quark being replaced by a down quark at the surface of the nugget, converting the proton to a neutron which can then escape. This process involves the exchange of a quark-antiquark pair and is a strong interaction process, but suppressed by the Zweig (OZI) rule. The overall rate of charge-exchange verse annihilation interactions is amplified by the high probability of reflection from the quark-matter boundary, which results in multiple bounces before annihilation.

A better understanding of the details concerning the interaction between the proton and the quark-matter boundary is required to quantitatively predict the ratios of the rate of charge-exchange to the rate of annihilation and thus to confirm or rule out the suppression factor $f \sim 0.1$–0.5 required to explain the relative strengths of the observed 511 keV and diffuse ~ 10 keV x-ray emissions seen from the core of the Galaxy [4]. This requires an estimate of the rates of reflection, annihilation, and charge-exchange; the elasticity of collisions; and the energy loss through scattering.

We emphasize that the corresponding calculations do not require any new physics: everything is rooted firmly in QED and QCD. They do, however, require solving the many-body physics of the strong interaction including the incident nucleons and the quark antimatter interface (the phase of which may be quite complicated). A full calculation is thus very difficult, requiring insight into high-density QCD: estimates can probably be made using standard models of nuclear matter for the core, but are beyond the scope of the present paper.

In any case, the nucleus will certainly deposit its charge on the antinugget, and one may neglect the interactions with neutral ISM components for the purpose of establishing charge neutrality.

Instead, we must consider the charged components. Using the same argument (11) one can see that the

[8] It is well known from quantum mechanics that any sufficiently sharp transition has a high probability of reflection of low energy particles.

Coulomb barrier of the charged nuggets will be high enough to prevent electrons from reaching the electrosphere in all but the very hot ionized medium (VHIM), which occupies only a small fraction of the ISM in the core (see [42] for example). Protons however, will be able to reach the core to annihilate with a cross-section $\sim 4\pi R^2$ (this is not substantially affected by the charge). Thus, positive charge can be deposited at a rate $\sim 4\pi R^2 v_{N+,\text{ISM}} n_{N+,\text{ISM}}$ where $n_{N+,\text{ISM}}$ is the density of the ionized components in the ISM, which is typically 10^{-1} to 10^{-2} of the total density $n_{\text{ISM}} \sim 1\ \text{cm}^{-3}$

This rate of positive charge accumulation must match the evaporation rate of the positrons from the electrosphere (see Eq. (7)), giving the boundary conditions (8b), and the resulting charges summarized in Table I.

Note that the rate of evaporation is much less than the rate of proton annihilation and carries only ~ 1 eV of every per particle compared to the nearly 2 GeV of energy deposited. Thus, evaporation does not significantly cool the nuggets: the thermal radiation from the Boltzmann regime discussed in [5] dominates.

IV. DIFFUSE GALACTIC EMISSIONS

Previous discussions of quark (anti)nugget dark matter considered the electrosphere in only two limiting cases: the inner high-density ultra-reletivistic regime and the outer low density Boltzmann regime. While this analysis was sufficient to qualitatively discuss the different components of the spectrum, it did not allow for their comparison in any level of detail. In particular, comparing the relative strengths of the 511 keV line emission with that of the MeV continuum required introducing a phenomenological parameter $\chi \approx 0.1$ [6] to expressed the relative rates of direct annihilation to positronium formation. This parameter is sensitive to the density profile at all scales. Using the detailed numerical solutions of the previous section we can now directly compute the relative intensities of the two emissions and shall show that this value of χ is supported by a purely microscopic calculation rooted firmly in QED and well-understood many-body physics. The agreement between the calculated value of χ and the phenomenological value required to fit the observations provides another important and non-trivial test of our dark-matter proposal.

A. Observations

1. The 511 keV Line

The SPI on the INTEGRAL satellite has detected a strong 511 keV signal from the galactic bulge [43]. A spectral analysis shows this to be consistent with low momentum e^+e^- annihilation through a positronium intermediate state: About one quarter of positronium decays emit two 511 keV photons, while the remaining three quarters will decay to a three photon state producing a continuum below 511 keV; Both emissions have been seen by SPI with the predicted ratios.

The 511 keV line is strongly correlated with the galactic centre with roughly 80% of the observed flux coming from a circle of half angle 6°. There also appears to be a small asymmetry in the distribution oriented along the galactic disk [44].

The measured flux from the galactic bulge is found to be $d\Phi/d\Omega \simeq 0.025$ photons $\text{cm}^{-2}\ \text{s}^{-1}\ \text{sr}^{-1}$ [45]. After accounting for all known galactic positronium sources the 511 keV line seems too strong to be explained by standard astrophysical processes. These processes, as we understand them, seem incapable of producing a sufficient number of low-momentum positrons. Several previous attempts have been made to account for this positron excess. Suggestions have included both modifications to the understood spectra of astrophysical objects or positrons which arise as a final state of some form of dark matter annihilation. At this time there is no conclusive evidence for any of these proposals.

If we associate the observed 511 keV line with the annihilation of low momentum positrons in the electrosphere of an antiquark nugget, these properties are naturally explained: The strong peak at the galactic centre and extension into the disk must arise because the intensity follows the distribution $\rho_V(r)\rho_{DM}(r)$ of visible and dark matter densities. No synchrotron emission will occur as the positrons are simply an integral part of the nuggets rather than being produced at high energies with only the low-energy components exposed for emission.

2. Diffuse MeV scale emission

The other component of the galactic spectrum we discuss here is the diffuse continuum emission in the 1 – 30 MeV range observed by SPI on the COMPTEL satellite. The interpretation of the spectrum in this range is more complicated that the 511 keV line as several different astrophysical processes contribute.

The conventional explanation of these diffuse emissions is that of gamma rays produced by the scattering of cosmic rays off of the interstellar medium, and while detailed studies of cosmic ray processes provide a good fit to the observational data over a wide energy range (from 20 MeV up to 100 GeV), the predicted spectrum falls short of observations by roughly a factor of two in the 1–20 MeV range [46].

Background subtraction is difficult, however, and especially obscurs the spatial distribution of the MeV excess. However, the excess seems to be confined to the inner galaxy ($l = 330^0 - 30^0$, $|b| = 0^0 - 5^0$), [46] with a negligible excess from outside of the galactic centre.

3. Comparison

As our model predicts both of these components to have a common source, a comparison of these emissions provides a stringent tests of the theory. In particular, the morphologies, spectra, and relative intensities of both emissions must be strongly related.

The inferred spatial distribution of these emissions is consistent – both are concentrated in the galactic core – but this is not a very stringent test due to the poor spatial resolutions of the present observations. The prediction remains firm: if the morphology of the observations can be improved, then a full subtraction of known astrophysical sources should yield a diffuse MeV continuum with spatial morphology identical to that of the 511 keV.

Present observations, however, do allow us to test the intensity and spectrum predicted by the quark nugget dark matter model. The model predicts the intensity to be proportional to the 511 keV flux. Therefore, the INTEGRAL data may be used to fix the total diffuse emission flux, removing the uncertainties associated with the line of sight averaging which is the same for both emissions.

The resulting spectrum and intensity were previously discussed in [28] and [6], but the 511 keV line emission was estimated using the low-density Boltzman approximation while the MeV emissions were estimated using the high-density ultrarelativistic approximation. The proportionality factor linking the two, however, was treated as a phenomenological parameter χ which required a value of $\chi \approx 0.1$ [6] in order to explain the observations.

Here, equipped with a complete density profile, we calculate the value of this parameter from first principles showing that it is indeed consistent with the observations, providing yet another highly non-trivial verification of the quark antimatter nugget dark matter proposal.

B. Annihilation rates

The basic picture is as follows: As incident electrons enter the electrosphere of positrons, the dominant annihilation process is through positronium formation: the subsequent annihilation produces the 511 keV emission. As the remaining electrons penetrate more deeply, they encounter a higher density of more energetic positrons and direct annihilation eventually becomes the dominant process. The maximum photon energy in this process is set by the Fermi energy of the electrosphere and will be at the MeV scale. In the following section we integrate the rates for these two processes over the complete density profile, allowing us to predict the relative intensities and spectral properties of the emissions.

1. Positronium Formation

In principle, we only need to know the e^+e^- annihilation cross-section at all centre of mass momenta. At high energies, this is perturbative and one can use the standard QED result for direct $e^+e^- \to 2\gamma$ emission. At low energies, however, one encounters a strong resonance due to the presence of a positronium state the greatly enhances the emission. This resonance renders a perturbative treatment invalid and must be dealt with specially, thus we consider these as two separate processes. Our presentation here will be abbreviated: details may be found in [28].

While the exact positronium formation rate – summed over all excited states – is not well established, it is clear that the rate will fall off rapidly as the centre of mass momentum moves away from resonance. A simple scatting calculation implies that for momenta $p > m\alpha$ the formation rate falls as $\sim p^{-4}$. To estimate the rate, we thus make a cutoff at $q \approx m\alpha$ as the upper limit for positronium formation: for large center of mass momenta we use the perturbative direct annihilation approximation. The scale here is set by the Bohr radius $a_b = 2(m\alpha)^{-1}$ for the positronium bound state: If a low momentum e^+e^- pair pass within this distance, then the probability of forming a bound state becomes large, with a natural cross section $\sigma_{Ps} \sim \pi a_b^2$. The corresponding rate is

$$\Gamma_{Ps} = \int_{p \lesssim q} v\sigma_{Ps} n(p) \frac{\mathrm{d}^3 p}{(2\pi)^3} \sim \frac{4v}{m^2\alpha^2} \begin{cases} n\pi & p_F \lesssim q \\ \frac{q^3}{3\pi} & p_F \gtrsim q. \end{cases} \quad (12)$$

where $n(p)$ is the momentum distribution of the positrons in the electrosphere, and $v \sim \alpha$ is the incoming electron velocity. The second expression represents the two limits (valid at low temperature): a) of low-density when the Fermi momentum $p_F \lesssim q$ and all states participate, resulting in a factor of the total density n, and b) of high density where the integral is saturated by $q^3/3\pi^2 \approx (m\alpha)^3/3\pi^2$.

As discussed in Sec. III C, electrons will only be able to penetrate the charged antimatter nuggets if they are bound in neutral objects. This complicates the analysis slightly, but the binding energy – on the eV scale – will not significantly alter the qualitative nature of our estimates. For a precision test of the emission properties, this will need to be accounted for. Here we include bands comprising $\pm 10\%$ relative variation in the overall positronium annihilation rate to show the sensitivity to this uncertainty.

2. Direct Annihilation Rates

While positronium formation is strongly favoured at low densities due to its resonance nature, deep within the electrosphere the rapidly growing density of states at large momentum values result in a cross-section characterized by the perturbative direct annihilation process.

Conceptually one can think of an incident galactic electron first moving through a Fermi gas of positrons with roughly atomic density with a relatively large probability of annihilation through positronium to 511 keV photons. A small fraction survive to penetrate to the inner high density region where direct annihilation dominates. The surviving electrons then annihilate with a high energy positron near to the inner quark-matter surface releasing high energy photons. The spectrum of these annihilation events will be a broad continuum with an upper cutoff at an energy scale set by Fermi energy of the positron gas at the maximum penetration depth of the electrons. The spectral density for direct e^+e^- annihilation at a given chemical potential was calculated in [6]:

$$\frac{dI(\omega,\mu)}{d\omega dt} = \int dn_p(\mu)\, v_p(\mu) \frac{d\sigma(p,\omega)}{d\omega} \tag{13}$$

$$= \int \frac{d^3p}{(2\pi)^3} \frac{2}{1+e^{(\mu-E_p)/T}} \frac{p}{E_p} \frac{d\sigma(p,\omega)}{d\omega} \tag{14}$$

$$\frac{d\sigma(p,\omega)}{d\omega} = \frac{\pi\alpha^2}{mp^2}\left[\frac{-(3m+E_p)(m+E_p)}{(m+E_p-\omega)^2} - 2 + \frac{\frac{1}{\omega}(3m+E_p)(m+E_p)^2 - (\frac{m}{\omega})^2(m+E_p)^2}{(m+E_p-\omega)^2}\right],$$

where $E_p = \sqrt{p^2+m^2}$ is the energy of the positron in the rest frame of the incident (slow-moving) electron and ω is the energy of the produced photons. The annihilation rate at a given density, $\Gamma_{\rm dir}(n_\mu)$, is obtained by integrating over allowed final state photon momentum. This was previously done in the $T \to 0$ limit where the integral may be evaluated analytically, at non-zero temperatures the rate must be evaluated numerically.

C. Spectrum and Branching Fraction

To determine the full annihilation spectrum we first determine the fraction of incident electrons that can penetrate to a given radius r in the electrosphere (see Fig. 3), then we integrate the emissions over all regions. Consider an incident beam of electrons with density n_∞ and velocity v. As discussed earlier, these electrons must be bound in neutral atoms – free electrons will be deflected by the net negative charge of the anti-nuggets – so the velocity will remain constant and will be set by the local velocity of atoms in the surround interstellar medium $v \sim 10^{-3}c$.

As they enter the electrosphere of positrons, the electrons will annihilate. The survival fraction $n_e(r)/n_\infty$ will thus decrease with a rate proportional to $\Gamma(r) = \Gamma_{Ps}(r) + \Gamma_{\rm dir}(r)$ which depends on the local density profile $n[\mu(r)]$ calculated in section III B:

$$\frac{dn_e(r)}{dt} = v^{-1}\frac{dn_e(r)}{dr} = -\Gamma(r)v^{-1}n_e(r). \tag{15}$$

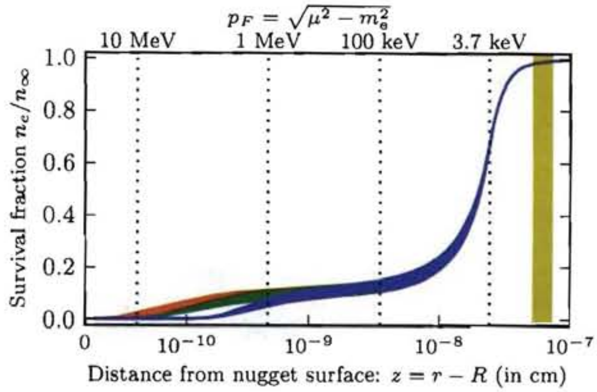

FIG. 3: (Colour online) Electron survival fraction, $n_e(r)/n_\infty$ (16) of an incoming electron with velocities $v = 0.01c$ (red), $v = 0.005c$ (green) and $v = 0.001c$ (blue) from left to right respectively. The thickness of the bands includes a $\pm10\%$ variation in the positronium annihilation rate (12). The local Fermi momentum p_F is shown along the top and with vertical dotted lines including the cutoff scale $q \approx 3.7$ keV from (12). The yellow shaded Boltzmann region and the abscissa scaling are the same as in the top of Fig. 1. Note that annihilation happens well within the electrosphere, so the finite size of the nugget is irrelevant.

Integrating (15), we obtain the survival fraction:

$$\frac{n_e(r)}{n_\infty} = \exp\left(-\int_r^\infty dr\, v^{-1}\Gamma(r)\right). \tag{16}$$

This is shown in Fig. 3. One can clearly the that in the outer electrosphere, positronium formation – independent of v – dominates the annihilation. Once the density is sufficiently high ($p_F \gtrsim 1$ MeV), the direct annihilation process dominates, introducing a dependence on the velocity v of the incident particle.

Two other features of Fig. 3 should be noted: First note the value of the survival fraction $\chi \sim 0.1$ at which direct-annihilation dominates (see Eq. 19). This is the value that was determined phenomenologically in [6] in order to explain the relative intensities of the 511 keV and direct annihilation spectra. Here this value results naturally from a direct microscopic calculation in a highly nontrivial manner that depends on the structure of the density provide at all scales up to $p_F = 1$ MeV. Second, note that the rapid increase in density near the core quickly extinguishes any remaining electrons. As such, even if the chemical potential at the surface is larger – $\mu_R \sim 100$ MeV or so – virtually no galactic electrons penetrate deeply enough to annihilate at these energies. For non-relativistic electrons the maximum energy scale for emission is quite generally set at the ~ 20 MeV scale, depending slightly on v.

Having established the survival fraction as a function of height it is now possible to work out the spectral density that will arise from the e^+e^- annihilations. At a given height we can express the number of annihilations through a particular channel as,

$$\frac{\mathrm{d}n}{\mathrm{d}r} = n_e(r)v^{-1}\Gamma(r). \tag{17}$$

Integrating this expression over all heights will then give the total fraction of annihilation events proceeding via positronium f_{511}, and via direct annihilation-annihilation f_{MeV}. (The numerical values are given for $q = m\alpha$ and are quite insensitive to v.)

$$f_{511} = \int_R^\infty \mathrm{d}r\, \frac{n_e(r)}{n_\infty} v^{-1}\Gamma_{Ps}(r) \approx 0.9, \tag{18a}$$

$$f_{\mathrm{MeV}} = \int_R^\infty \mathrm{d}r\, \frac{n_e(r)}{n_\infty} v^{-1}\Gamma_{\mathrm{dir}}(r) \approx 0.1. \tag{18b}$$

Note that in both cases, the overall normalization depends only on the total rate of electron collisions with dark matter through vn_∞. As such, the ratio of 511 keV photons to MeV continuum emission emission is independent of the relative densities (though it will show some dependence on the local electron velocity distribution). Numerically, with a $\pm 10\%$ variation in the positronium annihilation rate, we find

$$\chi = \frac{f_{\mathrm{MeV}}}{f_{511}} \approx 0.05 - 0.2, \tag{19}$$

which is quite insensitive to the velocity v. This ratio was introduced as a purely phenomenological parameter in [6] to explain the observations. Here we have calculated this value from purely microscopic considerations, finding that for a wide range of nugget parameters, the required value $\chi \sim 0.1$ [6] arises quite generally.

We now have everything needed to compute the spectral density of the MeV continuum. The spectral density at a fixed chemical potential is given by Eq. (13): this must now be averaged along the trajectory of the incoming electron weighted by the survival fraction (16) and the time spent in the given region of the trajectory (set by the inverse velocity v^{-1}):

$$\frac{\mathrm{d}I_{\mathrm{total}}}{\mathrm{d}\omega} = \int_R^\infty \mathrm{d}r\, v^{-1} \frac{n_e(r)}{n_\infty} \frac{\mathrm{d}I(\mu(r))}{\mathrm{d}\omega\,\mathrm{d}t}. \tag{20}$$

The resulting spectrum is shown in Figure 4 and is sensitive to both the incoming velocity v (which will depend on the local environment of the antimatter nugget) and the overall normalization of the positronium annihilation rate (12). (The latter is fixed in principle, but requires a difficult in-medium calculation to determine precisely.) These two parameters are rather orthogonal. The velocity v determines the maximum depth of penetration, and hence the maximum energy of the emitted photons (as set by the highest chemical potential at the annihilation point): If the electron velocity is relatively low ($v < 100$ km/s $\approx 0.0003c$), almost all annihilations happen immediately and the MeV continuum will fall rapidly

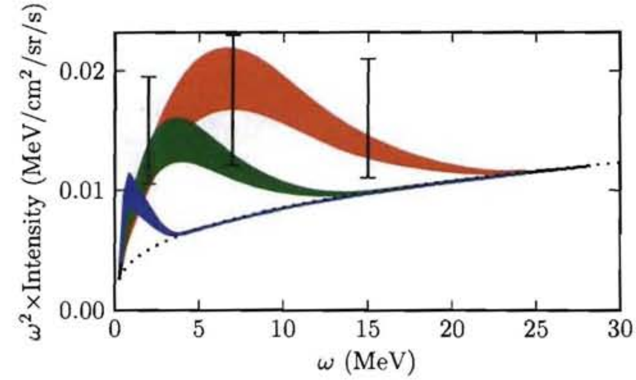

FIG. 4: (Colour online) Spectral density (scaled by ω^2 to compare with [46] of photons emitted by an electron annihilating on antiquark nuggets with incoming velocities $v = 0.01c$ (red), $v = 0.005c$ (green) and $v = 0.001c$ (blue) from right to left respectively, including the cosmic ray background determined in [46] (dotted line). The thickness of the bands includes a $\pm 10\%$ variation in the positronium annihilation rate (12). The overall normalization is fixed to the observationally unrelated 511 keV line as discussed below (21). The three error bars are the the COMPTEL data points. The observed spectrum will be an average of these exhibiting a dependence on the distributions of velocities v along the line of sight to the core of the galaxy.

beyond 5 MeV. As the velocity increases the electrons are able to penetrate deeper toward the quark surface and annihilate with larger energies. In contrast, the details of the positronium annihilation do not alter the spectral shape, but do alter the overall normalization.

1. *Normalization to the 511 keV line*

To obtain the observed spectrum, one needs to average (20) along the line of site over the varying matter and dark-matter density and velocity distributions. Neither of these is known very well, so to check whether or not the prediction is significant, we fix the average rate of electron annihilation with the observed 511 keV line which our model predicts to be produced by the same process. As the intensity of the 511 keV line (resulting from the two-photon decay of positronium in the $^1S_0$ state) has been measured by SPI/INTEGRAL along the line of sight toward the core of the galaxy (see [47] for a review), we can use this to fix the normalization of the MeV spectrum along the same line of sight. The total intensity is given in terms of Eq. (18a):

$$\frac{\mathrm{d}\Phi}{\mathrm{d}\Omega} = \frac{C}{4} f_{511} \sim 0.025 \frac{\text{photons}}{\text{cm}^2 \cdot \text{s} \cdot \text{sr}}, \tag{21}$$

where the factor of 4 accounts for the three-quarters of the annihilation events that decay via the $^3S_2$ channel (also measured, but not included in the line emission). This fixes the normalization constant $C \approx$

0.11 events $\cdot$ $cm^{-2}\cdot s^{-1}\cdot sr^{-1}$. The predicted contribution to the MeV continuum must have the same morphology and, thus, an integrated intensity along the same line of sight must have the same normalization factor. This normalization has been used in Figure 4 to compare the predicted spectrum with the unaccounted for excess emission detected by COMPTEL ([46]).

The exact shape of the spectrum will be an average of the components shown over the velocity distribution of the incident matter. Our process of normalization is unable to remove this ambiguity because the predicted 511 keV spectral properties are insensitive to this. It is evident, however, that MeV emission from dark matter nuggets could easily provide a substantial contribution to the observed MeV excess.

V. CONCLUSION

By solving the relativistic Thomas-Fermi equations, we determined the charge and structure of the positron electrosphere of quark antimatter nuggets that we postulate could comprise the missing dark-matter in our universe. We found the structure of the electrosphere to be insensitive to the size of the nuggets as long as they are large enough to be consistent with current terrestrial based detector limits, and hence can make unambiguous predictions about electron annihilation processes. Incidentally we note that the structure presented here – spanning from regimes of ultra-relativistic to non-relativistic densities – is the same as that of the electrosphere surrounding strange quark stars should they exist.

To test the dark-matter postulate further, we used the structure of this electrosphere to calculate the annihilation spectrum for incident electronic matter. The model predicts two distinct components: a 511 keV emission line from decay through a positronium intermediate and an MeV continuum emission from direct annihilation processes deep within the electrosphere. By fitting to the measured 511 keV line intensity seen from the core of the galaxy, our model makes a definite prediction about the intensity and spectrum of the MeV continuum spectrum without any additional adjustable model parameters.

A priori, there is no reason to expect that the predicted MeV spectrum should correspond to observations: typically two uncorrelated emissions are separated by many orders of magnitude. We find that the phenomenological parameter χ (19) required to explain the relative normalization of MeV emissions arises naturally from our microscopic calculation. This is highly non-trivial because it requires a delicate balance between the two annihilation processes from the semi-relativistic region of densities that is sensitive to the semi-relativistic self-consistent structure of the electrosphere outside the range of validity of the analytic ultra-relativistic and non-relativistic regimes. (See Figures 1 and 3).

If the predicted emission were several orders of magnitude too large, it would have ruled out our proposal. If the predicted emissions were too small, the proposal would not have been ruled out, but would have been much less interesting. Instead, we are left with the intriguing possibility that both the 511 keV spectrum and much or the MeV continuum emission arise from the annihilation of electrons on dark antimatter nuggets. While not a smoking gun – at least until the density and velocity distributions of matter and dark-matter are much better understood – this provides another highly non-trivial test of the proposal that, a priori, could have ruled it out.

Acknowledgments

MMF would like to thank George Bertsch, Aurel Bulgac, Sanjay Reddy, and Rishi Sharma for useful discussions.

[1] A. R. Zhitnitsky, JCAP **10**, 010 (2003), arXiv:hep-ph/0202161.

[2] D. H. Oaknin and A. Zhitnitsky, Phys. Rev. D **71**, 023519 (2005), arXiv:hep-ph/0309086.

[3] A. Zhitnitsky, Phys. Rev. **D74**, 043515 (2006), arXiv:astro-ph/0603064.

[4] M. M. Forbes and A. R. Zhitnitsky, JCAP **0801**, 023 (2008), arXiv:astro-ph/0611506.

[5] M. M. Forbes and A. R. Zhitnitsky, Phys. Rev. D **78**, 083505 (2008), 0802.3830.

[6] K. Lawson and A. R. Zhitnitsky, JCAP **0801**, 022 (2008), arXiv:0704.3064 [astro-ph].

[7] E. Witten, Phys. Rev. D **30**, 272 (1984).

[8] R. D. Peccei and H. R. Quinn, Phys. Rev. **D16**, 1791 (1977).

[9] S. Weinberg, Phys. Rev. Lett. **40**, 223 (1978).

[10] F. Wilczek, Phys. Rev. Lett. **40**, 279 (1978).

[11] J. E. Kim, Phys. Rev. Lett. **43**, 103 (1979).

[12] M. A. Shifman, A. I. Vainshtein, and V. I. Zakharov, Nucl. Phys. **B166**, 493 (1980).

[13] M. Dine, W. Fischler, and M. Srednicki, Phys. Lett. **B104**, 199 (1981).

[14] A. R. Zhitnitsky, Sov. J. Nucl. Phys. **31**, 260 (1980).

[15] M. Srednicki (2002), arXiv:hep-th/0210172.

[16] K. van Bibber and L. J. Rosenberg, Phys. Today **59N8**, 30 (2006).

[17] S. J. Asztalos, L. J. Rosenberg, K. van Bibber, P. Sikivie, and K. Zioutas, Ann. Rev. Nucl. Part. Sci. **56**, 293 (2006).

[18] D. Kharzeev and A. Zhitnitsky, Nucl. Phys. **A797**, 67 (2007), arXiv:0706.1026 [hep-ph].

[19] C. Amsler, M. Doser, M. Antonelli, D. M. Asner, K. S.

Babu, H. Baer, H. R. Band, R. M. Barnett, E. Bergren, J. Beringer, et al. (Particle Data Group), Phys. Lett. **B667**, 1 (2008).
[20] M. M. Forbes and A. R. Zhitnitsky, in prep.
[21] E. T. Herrin, D. C. Rosenbaum, and V. L. Teplitz, Phys. Rev. D **73**, 043511 (2006), arXiv:astro-ph/0505584.
[22] E. S. Abers, A. K. Bhatia, D. A. Dicus, W. W. Repko, D. C. Rosenbaum, and V. L. Teplitz (2007), arXiv:0712.4300 [astro-ph].
[23] E. W. Kolb and M. S. Turner, *The Early Universe* (Westview Press, 5500 Central Avenue, Boulder, Colorado, 80301, 1994).
[24] J. Knödlseder, V. Lonjou, P. Jean, M. Allain, P. Mandrou, J.-P. Roques, G. Skinner, G. Vedrenne, P. von Ballmoos, G. Weidenspointner, et al., Astron. Astrophys. **411**, L457 (2003), arXiv:astro-ph/0309442.
[25] J. F. Beacom and H. Yüksel, Phys. Rev. Lett. **97**, 071102 (2006), arXiv:astro-ph/0512411.
[26] H. Yüksel, Nucl. Phys. B Proc. Suppl. **173**, 83 (2006), arXiv:astro-ph/0609139.
[27] D. H. Oaknin and A. R. Zhitnitsky, Phys. Rev. Lett. **94**, 101301 (2005), arXiv:hep-ph/0406146.
[28] A. Zhitnitsky, Phys. Rev. D **76**, 103518 (2007), arXiv:astro-ph/0607361.
[29] M. P. Muno et al., Astrophys. J. **613**, 326 (2004), arXiv:astro-ph/0402087.
[30] D. P. Finkbeiner, Astrophys. J. **614**, 186 (2004), arXiv:astro-ph/0311547.
[31] D. P. Finkbeiner, G. I. Langston, and A. H. Minter, Astrophys. J. **617**, 350 (2004), arXiv:astro-ph/0408292.
[32] D. P. Finkbeiner (2004), arXiv:astro-ph/0409027.
[33] D. Hooper, G. Zaharijas, D. P. Finkbeiner, and G. Dobler, Phys. Rev. D **77**, 043511 (2007), arXiv:0709.3114 [astro-ph].
[34] G. Dobler and D. P. Finkbeiner (2007), arXiv:0712.1038 [astro-ph].
[35] C. Alcock, E. Farhi, and A. Olinto, Astrophys. J. **310**, 261 (1986).
[36] C. Kettner, F. Weber, M. K. Weigel, and N. K. Glendenning, Phys. Rev. D **51**, 1440 (1995).
[37] K. S. Cheng and T. Harko, Astrophys. J. **596**, 451 (2003), arXiv:astro-ph/0306482.
[38] V. V. Usov, T. Harko, and K. S. Cheng, Astrophys. J. **620**, 915 (2005), arXiv:astro-ph/0410682.
[39] L. D. Landau and E. M. Lifshitz, *Quantum Mechanics: Non-relativistic theory*, vol. 3 of *Course of Theoretical Physics* (Butterworth-Heinemann, Oxford, 2003, c1977), 3rd ed.
[40] D. T. Cumberbatch, J. Silk, and G. D. Starkman, Phys. Rev. D **77**, 063522 (2008), arXiv:astro-ph/0606429.
[41] V. V. Usov, Phys. Rev. D **70**, 067301 (2004), arXiv:astro-ph/0408217.
[42] K. Ferrière, W. Gillard, and P. Jean, A&A **467**, 611 (2007), arXiv:astro-ph/0702532, URL http://dx.doi.org/10.1051/0004-6361:20066992.
[43] G. Weidenspointner, C. R. Shrader, J. Knödlseder, P. Jean, V. Lonjou, N. Guessoum, R. Diehl, W. Gillard, M. Harris, G. Skinner, et al., Astron. Astrophys. **450**, 1013 (2006), arXiv:astro-ph/0601673.
[44] G. Weidenspointner, G. K. Skinner, P. Jean, J. Knödlseder, P. von Ballmoos, G. Bignam, R. Diehl, A. W. Strong, B. Cordier, S. Schanne, et al., Nature **451**, 159 (2008).
[45] P. Jean et al., Astron. Astrophys. **407**, L55 (2003), arXiv:astro-ph/0309484.
[46] A. W. Strong, I. V. Moskalenko, and O. Reimer, Astrophys. J. **613**, 962 (2004), arXiv:astro-ph/0406254.
[47] G. Weidenspointner, G. Skinner, P. Jean, J. Knödlseder, P. von Ballmoos, R. Diehl, A. Strong, B. Cordier, S. Schanne, and C. Winkler, New Astronomy Reviews **52**, 454 (2008), ISSN 1387-6473, astronomy with Radioactivities. VI - Proceedings of International Workshop Held at Ringberg Castle of Max Planck Gesellschaft in Kreuth, Germany, 7-10 January 2008, URL http://www.sciencedirect.com/science/article/B6VNJ-4SSY91T-
[48] P. Hohenberg and W. Kohn, Phys. Rev. **136**, B864 (1964).
[49] E. Braaten, ApJ **392**, 70 (1992).
[50] E. H. Lieb and B. Simon, Phys. Rev. Lett. **31**, 681 (1973).

Appendix A: Density Functional Theory

We start with a Density Functional Theory (DFT) formulated in terms of the thermodynamic potential:

$$\Omega = \sum_i 2f_i \int \mathrm{d}^3r\ \psi_i^\dagger(r)(\epsilon_{-i\hbar\vec{\nabla}} - \mu)\psi_i(r) + \\ + \int \mathrm{d}^3r V_{\text{ext}}(r)n(r) + \int \mathrm{d}^3r\ \varepsilon_{xc}\Big[n(r)\Big]n(r) + \\ + \frac{4\pi e^2}{2}\int \mathrm{d}^3r'\ \frac{n(r)n(r')}{\|r-r'\|} - T\sum_i f_i \ln f_i, \quad \text{(A1a)}$$

where $\epsilon_p = \sqrt{p^2+m^2}$ is the relativistic energy of the electrons, $\varepsilon_{xc}(n)$ is the exchange energy, and the density is

$$n(r) = 2\sum_i f_i\psi_i^\dagger(r)\psi_i(r), \quad \text{(A1b)}$$

where we have explicitly included the spin degeneracy, and used relativistic units where $\hbar = c = 1$ and $e^2 = \alpha$.

We vary the potential with respect to the occupation numbers f_i and the wavefunctions ψ_i subject to the constraints that the wavefunctions be normalized,

$$\int \mathrm{d}^3r\ \psi_i^\dagger(r)\psi_j(r) = \delta_{ij}, \quad \text{(A1c)}$$

and that the occupation numbers satisfy Fermi-Dirac statistics.[9] This yields the Kohn-Sham equations for the electronic wavefunctions:

$$\Big[\epsilon_{-i\hbar\nabla} - \mu + V_{\text{eff}}(r)\Big]\psi_i(r) = E_i\psi_i(r), \quad \text{(A2a)}$$

$$f_i = \frac{1}{1+e^{E_i/T}}. \quad \text{(A2b)}$$

where (we take e to be positive here)

$$V_{\text{eff}}(r) = e\phi(r) + V_{\text{ext}}(r) + \varepsilon_{xc}[n(r)] + n(r)\varepsilon'_{xc}[n(r)] \quad \text{(A2c)}$$

and

$$\phi(r) = 4\pi e\int \mathrm{d}^3\tilde{r}\frac{n(r+\tilde{r})}{\|\tilde{r}\|} \quad \text{(A2d)}$$

is the electrostatic potential, which obeys Poisson's equation,

$$\nabla^2\phi(r) = -4\pi e n(r). \quad \text{(A2e)}$$

[9] This is most easily realized by introducing the single-body density matrix $\boldsymbol{\rho} = \mathbf{1} - \mathbf{C}\boldsymbol{\rho}^T\mathbf{C}$ where $\mathbf{C}$ is the charge-conjugation matrix.

1. Thomas-Fermi Approximation.

If the effective potential $V_{\text{eff}}(r)$ varies sufficiently slowly, then it is a good approximation to replace it locally with a constant potential. The Kohn-Sham equations thus become diagonal in momentum space, $i \equiv k$, $\psi_k \propto e^{ikr}$ and may be explicitly solved:

$$E_k(r) = \epsilon_k - \mu + V_{\text{eff}}(r),$$
$$n(r) = 2\int \frac{\mathrm{d}^3k}{(2\pi)^3}\left(\frac{1}{1+e^{E_k(r)/T}} - \frac{1}{1+e^{-E_k(r)/T}}\right),$$

were we have also explicitly included the contribution from the antiparticles. We piece these homogeneous solutions together at each point r and find the self-consistent solution that satisfies Poisson's equation. This approximation is a relativistic generalization of the Thomas-Fermi approximation.

In principle, the DFT method is exact [48], however, the correct form for ε_{xc} is not known and could be extremely complicated. Various successful approximations exist but for our purposes we may simply neglect this. The weak electro-magnetic coupling constant $\alpha \sim 1/137$ and Pauli exclusion principle keeps the electrons sufficiently dilute that the many-body correlation effects can be neglected until the density is high in the sense that $\alpha^2 n \sim \alpha^2\mu^3/3\pi^3 \gtrsim m^3$, which corresponds to $\mu \gtrsim 50$ MeV.

Near the core, many-body correlations may become quantitatively important: For example, the effective mass of the electrons in the gas is increased by about 20% when $\mu \approx 25$ MeV and doubles when $\mu \approx 100$ MeV (see for example [49]). These effects, however, will not change the qualitative structure, and can be quite easily taken into account if higher accuracy is required. We also note that formally, the Thomas-Fermi approximation is only valid for sufficiently high densities. However, it gives correct energies within factors of order unity for small nuclei [39] and is known to work substantially better for large nuclei [50]. As long as we do not attempt to use it in the extremely low-density tails, it should give an accurate description here.

2. Analytic Solutions

There are several analytic solution available if we consider the one-dimensional approximation, neglecting the curvature term $2\mu'(r)/r$ in (5), which is valid close to the nugget where $z = r - R \ll R$, the distance from the nugget core, is less than the radius of the nugget.

a. *Ultra-Relativistic Regime*

The first is the ultra-relativistic approximation where μ and/or T are much larger than m and the limit $m \to 0$

can be taken. In this case, we may explicitly evaluate (see also [36–38]), [10]

$$n[\mu, T]_{m\ll\mu,T} = \frac{\mu^3}{3\pi^2} + \frac{\mu T^2}{3}. \tag{A6}$$

In the domain wall approximation, this admits and exact solution with a typical length scale of z_{UR}:

$$\mu(z,T) = \frac{T\pi\sqrt{2}}{\sinh\left[2T\sqrt{\frac{\alpha\pi}{3}}(z+z_T)\right]}, \tag{A7}$$

$$z_{\text{UR}} = \frac{1}{2T}\sqrt{\frac{3}{\alpha\pi}}\sinh^{-1}\left(\frac{T\pi\sqrt{2}}{\mu_R}\right). \tag{A8}$$

In our case, $T \sim 1$ eV $\ll m$ so we can also take the $T \to 0$ limit to obtain (9):

$$n_{\text{UR}}(z) \approx \frac{\mu_R^3}{3\pi^2(1+z/z_{\text{UR}})^3}, \quad z_{\text{UR}} \approx \mu_R^{-1}\sqrt{\frac{3\pi}{2\alpha}}. \tag{A9}$$

This solution persists until $\mu \approx m$, which occurs at a distance

$$z_B \approx z_{\text{UR}}\left(\frac{\mu_R}{m} - 1\right) \approx m^{-1}\sqrt{\frac{3\pi}{2\alpha}}. \tag{A10}$$

b. *Boltzmann Regime*

Once the chemical potential is small enough that $e^{\mu/T} \ll e^{m/T}$, we may neglect the degeneracy in the system, and write

$$n[\mu]|_{\exp(\mu/T)\ll\exp(m/T)} \approx n_0 e^{\mu/T}. \tag{A11}$$

This occurs for a density of about

$$n_B \approx \left(\frac{mT}{2\pi}\right)^{3/2} \tag{A12}$$

and lower. If the one-dimensional approximation is still valid, then another analytic solution may be found:

$$n(z) = \frac{n_B}{\left(1+\frac{z-z_B}{z_\alpha}\right)^2}, \qquad z_\alpha = \sqrt{\frac{T}{2\pi\alpha n_B}} \tag{A13}$$

from which we obtained (10). The shift z_B must be determined from the numerical profile at the point where $n(z_B) = n_B$. Note that $z_\alpha \ll z_B$, so this regime is valid and persists until $z \sim 0.1R$, at which point the one-dimensional approximation breaks down. It is in this Boltzmann regime where most of the important radiative processes take place [5].

3. Numerical Solutions

The main technical challenge in finding the numerical solution is to deal effectively with the large range of scales: $T \sim 1$ eV $\ll m \sim 500$ keV $\ll \mu_R \sim 25$ MeV. For example, the density distribution (4b) is prone to round-off error, but the integral can easily be rearranged to give a form that is manifestly positive:

$$n[\mu] = \frac{1}{\pi^2}\int_0^\infty \mathrm{d}p\, \frac{p^2\sinh\left(\frac{\mu}{T}\right)}{\cosh\left(\frac{\sqrt{p^2+m^2}}{T}\right) + \cosh\left(\frac{\mu}{T}\right)}. \tag{A14}$$

The derivative may also be safely computed. Let

$$A = \frac{\sqrt{p^2+m^2}}{T}, \qquad B = \frac{\mu}{T}, \tag{A15}$$

to simplify the expressions. These can each be computed without any round-off error. The first derivative presents no further difficulties:

$$\dot{n}[\mu] = \frac{1}{T\pi^2}\int_0^\infty \mathrm{d}p\, p^2 \frac{1+\cosh A\cosh B}{(\cosh A + \cosh B)^2}. \tag{A16}$$

The differential equation is numerically simplified if we change variables to logarithmic quantities. We would also like to capture the relevant physical characteristics of the solution, known from the asymptotic regimes. Close to the nugget, we have $\mu = \mu_R/(1+z/z_0)$, we introduce an abscissa logarithmic in the denominator

$$a = \ln\left(1+\frac{z}{z_0}\right) = \ln\left(1+\frac{r-R}{z_0}\right). \tag{A17}$$

The dependent variable should be logarithmic in the chemical potential, so we introduce $b = -\ln(\mu/\mu_0)$. We thus introduce the following change of variables

$$r = R + z_0(e^a - 1), \qquad \mu = \mu_0 e^{-b}, \tag{A18a}$$

$$a = \ln\left(1+\frac{r-R}{z_0}\right), \qquad b = -\ln\frac{\mu}{\mu_0}. \tag{A18b}$$

With the appropriate choice of scales z_0 describing the typical length scale at the wall $r = R$ and $\mu_0 \sim \mu_R$, these

---

[10] In this limit, then integrals have a closed form:

$$\begin{aligned} n[\mu,T]_{m\ll\mu,T} &= \\ &= \frac{1}{\pi^2}\int_0^\infty \mathrm{d}p\left[\frac{p^2}{1+e^{(p-\mu)/T}} - \frac{p^2}{1+e^{(p+\mu)/T}}\right] = \\ &= \frac{T^3}{\pi^2}\int_0^\infty \mathrm{d}x\left[\frac{x^2}{1+e^{x-\mu/T}} - \frac{x^2}{1+e^{x+\mu/T}}\right] = \\ &= \frac{-T^3}{\pi^2}\Gamma(3)\left[\mathrm{Li}_3(-e^{\mu/T}) - \mathrm{Li}_3(-e^{-\mu/T})\right] \end{aligned} \tag{A4}$$

where $\mathrm{Li}_s(z)$ is the Polylogarithm

$$\mathrm{Li}_s(z) = \sum_{k=1}^\infty \frac{z^k}{k^s}. \tag{A5}$$

form quite a smooth parametrization. The resulting system is

$$\ddot{b}(a) = \dot{b}(a)\left(\dot{b}(a) + \frac{R - z_0 - z_0 e^a}{R - z_0 + z_0 e^a}\right) + \\ - 4\pi\alpha z_0^2 e^{2a}\frac{n[\mu]}{\mu}. \quad (A19)$$

Appendix B: Debye Screening In the Electrosphere

Here we briefly discuss the plasma properties inside of the nugget's electrosphere. The main point is that the Debye screening length λ_D is much smaller than the typical de Broglie wavelength $\lambda = \hbar/p$ of electrons. Thus, the electric fields – although quite strong in the nugget's electrosphere – will not appreciably effect the motion of electrons within the electrosphere as the charge is almost completely screened on a scale $\sim \lambda_D$.

This screening effect was completely neglected in [40] which led them to erroneously conclude that all electrons will be repelled before direct annihilation can proceed. The overall charge I will repel incident electrons at long distances as discussed in section III C, but neutral hydrogen will easily penetrate the electrosphere, at which point the screening becomes effective, allowing the electrons to penetrate deeply and annihilate as discussed in section IV.

To estimate the screening of an electron, we solve the Poisson equation with a $\delta^3(r - r_0)$ function describing the electron at position r_0 (see also 2),

$$\nabla^2\phi(r) = -4\pi e\left[n(r) - \delta^3(r - r_0)\right] \tag{B1}$$

where $\phi(r)$ is the electrostatic potential and $n(r)$ is the density of positrons. As before, we exchange ϕ for μ, the effective chemical potential (3). Now let $n_0(r)$ and $\mu_0(r)$ be the solutions discussed in section III B without the potential $\delta^3(r - r_0)$. We may then describe the screening cloud by $\mu(r) = \mu_0(r) + \delta_\mu(r)$ and $n(r) = n_0(r) + \delta_n(r)$ where

$$\begin{aligned}\nabla^2\delta_\mu(r) &= 4\pi e^2\left[\delta_n(r) - \delta^3(r - r_0)\right]\\ &\approx 4\pi\alpha\left[\frac{\partial n[\mu]}{\partial\mu}\delta_\mu(r) - \delta^3(r - r_0)\right]\end{aligned} \tag{B2}$$

where $n[\mu]$ is given by (4b). If the density is sufficiently large compared to the screening cloud deviations, we may take $\partial n/\partial\mu$ to be a constant, in which case we may solve (B2) analytically with the boundary conditions:

$$\lim_{r\to r_0}\delta_\mu(r) = \frac{4\pi\alpha}{|r - r_0|}, \qquad \lim_{r\to\infty}\delta_\mu(r) = 0. \tag{B3}$$

This gives the standard Debye screening solution

$$\delta_\mu(r) = \frac{-4\pi\alpha}{|r - r_0|}\exp\left(-\frac{|r - r_0|}{\lambda_D}\right) \tag{B4}$$

where the Debye screening length is

$$\lambda_D^{-2} = 4\pi\alpha\frac{\partial n[\mu]}{\partial\mu}. \tag{B5}$$

On distances larger than λ_D, the charge of the electron is effectively screened. In particular, we can neglect the influence of the external electric field on motion of the electron if λ_D is small compared to the de-Broglie wavelength $\lambda = \hbar/p$ of the electrons:

$$1 \ll \frac{\lambda}{\lambda_D} \sim \frac{1}{mv}\sqrt{4\pi\alpha\frac{\partial n[\mu]}{\partial\mu}}. \tag{B6}$$

In the ultra-relativistic limit (A6), one has $\partial n/\partial\mu \approx \mu^2/\pi^2 + T^2/3$ whereas in the Boltzmann limit (A11), one has $\partial n/\partial\mu \approx n_0/T$.

The relevant electron velocity scales in our problem is $v \sim 10^{-3}c$ ($T \sim 1$ eV). This is the typical scale for electrons ionized from neutral hydrogen. For these electrons, one immediately sees that the screening becomes significant in the Boltzmann regime once the density is larger than

$$n_0 \gg \frac{m^2v^2T}{4\pi\alpha} \sim 0.1 n_B \tag{B7}$$

where $n_B = (mT/2\pi)^{3/2}$ is the typical density in the Boltzmann regime. The typical electric fields in this regime are $E \sim \nabla\phi \sim eT/2z_\alpha$ which yields an ionization potential of $V_{\text{ionize}} \sim eEa_0 \sim \alpha T a_0/2z_\alpha \sim 1$ meV $\ll$ 13 eV. Thus, the ionization of incoming hydrogen will not occur until the density is much larger, by which point the screening will be highly efficient. Contrary to the arguments presented in [40], electrons depositive via neutral hydrogen can easily penetrate deeply into the electrosphere producing the direct annihilation emissions discussed in section IV.

Finally, we point out that, in the ultra-relativistic regime, we may express (B6) in terms of the Fermi momentum:

$$\frac{\lambda}{\lambda_D} \sim \frac{p_F}{p}\sqrt{\frac{\alpha}{\pi}}. \tag{B8}$$

Thus, for highly energetic particles, screening is irrelevant. The would apply to the ~ 5 MeV positrons ejected from core of the nuggets that we argued are responsible for the diffuse 10 keV emission [4]. These see the full electric field which is responsible for their deceleration and ultimately for the emission of their energy in the 10 keV band. This point is somewhat irrelevant, however, as the positron electrosphere of the antimatter nuggets cannot screen a positive charge (screening is only efficient for particles of the opposite charge than the ion constituents).